

Numerical Simulation of Hypersonic Dynamic Stability Parameters: 7 Degrees Blunt Cone Mode Dynamic Derivative Supported Interference

Xu LIU^a, Hao HAN^{a,1} and Yi YOU^a

^aNaval Submarine Academy, Qingdao, China

ORCID ID: Hao HAN, <https://orcid.org/0000-0002-7685-2758>

Abstract. In hypersonic winds, special tests for dynamic stability parameters usually use a model tail to support forced vibration. Supporting disturbances under dynamic conditions may result in unsteady flow structures such as shock-induced separation, vortex motion and rupture. The nonlinear aerodynamic loads generated by such structures lead to difficult and complex techniques for supporting interference under dynamic conditions. In the paper, the numerical simulation of the tail support interference of the special wind tunnel test with dynamic three-dimensional unsteady N-S equation is carried out. Numerical simulation and experimental comparison of three different supports were carried out for the 7° blunt cone model. For the static aerodynamic coefficient, the greatest influence of the support disturbance is the drag coefficient. The pitch damping derivative under dynamic conditions is very different, and the support interference is up to 40%. Support interference under dynamic conditions is much more complicated than static conditions. The control law of support interference under static conditions cannot be directly applied to dynamic unsteady conditions. It is considered that the tail support of this form design has less dynamic flow field interference to the aspirating hypersonic vehicle and meets the needs of the dynamic wind tunnel test.

Keywords. Hypersonic, Support interference, Numerical simulation, Dynamic stability parameters

1. Introduction

In hypersonic wind tunnels, most of them use forced vibration method with tail support to carry out dynamic derivative experiments [1]. Supporting interference is one of the important sources of dynamic derivative error. For some shapes, the influence of supporting interference on the aerodynamic force of the model far exceeds the interference effect of the wall. In the hypersonic wind tunnel, the tail branch interference is mainly reflected in the interference of the resistance, especially the bottom resistance measurement, and the bottom resistance correction is a problem that has not been solved well in the hypersonic wind tunnel test. Uselton pointed out [2] that the influence of the

¹Corresponding author, Hao HAN, Naval Submarine Academy, Qingdao, China. OICID: 0000-0002-7685-2758

tail support on the dynamic aerodynamic force of the blunt cone far exceeds the static situation. When it comes to the nonlinear aerodynamic loads caused by shock-induced separation, vortex motion and rupture, the study of support interference under dynamic conditions is a difficult and technically complex subject. For the special experiments such as the dynamic derivative, there has not been any systematic support interference correction research. At present, under the background of the rapid development of hypersonic vehicle technology, for hypersonic complex aircraft, especially the body propulsion integrated aircraft including inflow, it is urgent to carry out support interference research for the special experiment of dynamic derivative [3].

The correction of support interference mainly includes test correction method, engineering correction method and numerical calculation method. The test correction method uses the auxiliary bracket and the superposition method to measure the interference of the main (false) support. This method has been used for many years. Regardless of the type of support system, regardless of the high and low speed wind tunnels, regardless of the static and dynamic tests, the superposition method is used to determine the support. Interference, but in practice it has been found that measurements are unreasonable in some cases, which often occurs when separate flows, large disturbances, or unsteady flows occur [4]. Literature [5] reviewed the scaffold interference in dynamic experimental studies. GSTaylor et al. studied the dynamic scaffold interference of delta wing by water tunnel test [6], and the results show that the experimental correction of the dynamic derivative support interference under dynamic unsteady conditions. The method has high cost, and the test conditions are limited, and the method of assisting the support with virtual struts is generally adopted. Support interference correction is performed, and it is difficult to deduct secondary interference [7].

The engineering correction method has great limitations. The engineering correction method is not reliable when the test model and the bracket form are far from the model and bracket form of the known bracket interference. The literature [8] proposes an engineering estimation correction method for high-speed tail strut interference. The tail support system has little interference with the lift of the conventional force measurement model and can be corrected. The influence of the strut on the resistance of the model is mainly the influence on the rear body resistance of the model. It depends on the geometry of the rear body of the model, the geometric parameters of the strut, the incoming Mach number and the Reynolds number. However, there are no reliable engineering estimation methods for special tests such as dynamic derivatives under dynamic unsteady conditions [9].

The numerical calculation method considering flow nonlinearity and unsteady effect has high precision and is not affected by disturbance factors such as model motion, and is an important development direction of support interference correction [10]. At present, most studies use numerical calculation methods to carry out conventional static aerodynamic support interference correction, and systematic support interference correction studies for dynamic derivative special experiments are rare [11]. In this paper, based on the 7° blunt cone model [12], the three-dimensional unsteady N-S equation is used to study the support interference of the length of the beam, and the experimental data of static aerodynamic force and dynamic derivative are compared.

2. Calculation method

2.1. Computational Fluid Dynamics Formulation

Navier-Stokes (NS) equations are established based on the three conservation laws of physics: mass conservation, momentum conservation and energy conservation. The conserved integral form without volume force and external heat source in cartesian coordinate system is expressed as:

$$\frac{\partial}{\partial t} \int_{\Omega} \tilde{Q} d\tilde{V} + \oint_{\partial\Omega} (\tilde{F} - \tilde{F}_v) \cdot \tilde{n} d\tilde{S} = 0 \tag{1}$$

Superscript "~" is dimensional quantity, $\tilde{Q} = (\tilde{\rho}, \tilde{\rho}\tilde{u}, \tilde{\rho}\tilde{v}, \tilde{\rho}\tilde{w}, \tilde{\rho}\tilde{e})^T$ as conservation variables, $\tilde{\rho}, (\tilde{u}, \tilde{v}, \tilde{w}), \tilde{e}$ are respectively density, the speed of the components in the Cartesian coordinate system and unit mass gas can always; Ω and $\partial\Omega$ are the integral domain and boundary of integral domain respectively; \tilde{n} is the normal vector outside the boundary surface; \tilde{F} and \tilde{F}_v are convective and viscous fluxes, respectively. Eq. (1) can also be written into the following conserved differential form:

$$\frac{\partial \tilde{Q}}{\partial t} + \frac{\partial \tilde{E}}{\partial x} + \frac{\partial \tilde{F}}{\partial y} + \frac{\partial \tilde{G}}{\partial z} = \frac{\partial \tilde{E}_v}{\partial x} + \frac{\partial \tilde{F}_v}{\partial y} + \frac{\partial \tilde{G}_v}{\partial z} \tag{2}$$

In the Eq. (2), $\tilde{E}, \tilde{F}, \tilde{G}$ and $\tilde{E}_v, \tilde{F}_v, \tilde{G}_v$ are the components of flow and viscous flux respectively.

In this paper, the space derivative term of the finite-volume discrete flow control system is adopted with the second-order windward NND format, and the time-solving efficiency and accuracy are improved by using the LU-SGS method with double time steps. The turbulence model adopts SA model based on engineering experience and dimensional analysis. The far field boundary adopts the reflection-free boundary condition of one-dimensional Riemann invariant applicable to dynamic boundary conditions. On the wall boundary, the velocity adopts the non-slip condition, the temperature adopts the adiabatic wall condition, and the pressure condition takes into account the influence of centrifugal force.

The airframe/propulsion integrator has complex wave system structure when flying at high speed. The shock wave and boundary layer interference inside the inlet can be distinguished by using a close calculating grid. The need for accurate simulation of aircraft under different working conditions is huge, with tens of millions of grids. Especially under the condition of dynamic motion, subiteration is needed to improve the time simulation accuracy of unsteady motion and unsteady flow, which greatly increases the computational cost. Therefore, this paper adopts the programming method of FORTRAN+MPI. In this paper, greedy algorithm is used to subdivide the computational grid to meet the requirement of load balance for the computational grid. This algorithm can be implemented by the following steps:

1. To calculate the global average calculation time T_{ave}

$$T_{ave} = \frac{\sum_{k \in G} N_k W}{\sum_j P_j} \tag{3}$$

In the Eq. (3), W is the number of floating-point operations on a single grid point, N_k is the number of grid cells in block k , P_j is the number of floating-point operations per second of processor j , and G is all grids. In addition, G_j is the grid that has been assigned to processor j , G_u and M_u are unallocated grids and number of blocks respectively.

2.To calculate processing time of each processor to the assigned grid T_j , Eq. (4):

$$T_j = \frac{1}{P_j} \sum_{k \in G_j} N_k W \tag{4}$$

3.To look for the fastest processor P_{fast} to compute the allocated grid and the largest unallocated grid block G_{large} , Eq. (5):

$$T_{fast} = \min(T_j) \quad N_{large} = \max_{k \in G_u}(N_k) \tag{5}$$

4.The computation time T_{large} required by the processor P_{fast} after the maximum grid block G_{large} is added, Eq. (6):

$$T_{large} = T_{fast} + \frac{N_{large}W}{P_{fast}} \tag{6}$$

5.To tell if the grid block G_{large} is divided, if $T_{large} > (1 + \epsilon)T_{ave}$, the maximum grid block G_{large} is divided into G_{assign} and G_{rest} , and the calculation time Eq. (7) is :

$$T_{assign} = T_{ave} - T_{fast}, \quad T_{rest} = T_{large} - T_{ave} \tag{7}$$

Tolerance ϵ is generally 0.01. G_{assign} is G_{large} , G_{rest} adding in unallocated grid G_u .

6.Assign the allocated grid block G_{large} to the processor P_{fast} and assign it to the allocated grid.

Check If the number of unallocated grid blocks, if $M_u > 0$,then the repeated process of 2-7, if $M_u = 0$, it means that the grid allocation is completed and the load balance is achieved.

2.2. Prediction Methods for Dynamic Derivatives

Dynamic stability parameters are the key aerodynamic parameters for the design of aircraft control system, boundary analysis of the occurrence of dynamic instability of aircraft and the study of the corresponding dynamic stability criterion. The acceleration derivative represents the delay effect of the aircraft doing sinking and floating motion or washing (up or down) and the time hysteresis characteristics of unsteady vortices. The rotation derivative represents the additional aerodynamic characteristics caused by local changes of the angle between the aircraft surface and incoming flow caused by the change of attitude angular velocity. The calculation methods of these dynamic stability parameters are given in this section, and the numerical validation is carried out in the next section.

The aerodynamic moment/ coefficients C_λ are the angle of attack α , sideslip angle β , rolling axis X_b , pitch axis Y_b , The functional of the angular velocity component p, q, r of the yaw axis Z_b . C_λ and the time being examined t is related to the history of the entire state of motion, which can be expressed as follow:

$$C_\lambda(t) = C_\lambda(\alpha(\xi), \beta(\xi), p(\xi), q(\xi), r(\xi)) \quad - \infty < \xi \leq t \tag{8}$$

For the sake of convenience but without loss of generality, the relationship between aerodynamic torque coefficient C_m and angle of attack $\alpha(\xi)$ is discussed, and Eq. (8) can be simplified as:

$$C_m(t) = C_m(\alpha(\xi)) \quad - \infty < \xi \leq t \tag{9}$$

Assume the aircraft before $\xi = 0$ is steady liner flight, angle of attack is α_0 , The following two forms are the motion state:

$$\alpha_1(\xi) = \begin{cases} \alpha(\xi) & 0 \leq \xi \leq \tau \\ \alpha(\tau) & \xi > \tau \end{cases} \tag{10}$$

$$\alpha_2(\xi) = \begin{cases} \alpha(\xi) & 0 \leq \xi \leq \tau \\ \alpha(\tau) + \Delta\alpha & \xi > \tau \end{cases} \tag{11}$$

In the Eqs. (10-11), ξ is the time coordinate, τ is a fixed time, when $\xi \leq \tau$, $\alpha_1 = \alpha_2$, when $\xi > \tau$, $\alpha_1 - \alpha_2 = \Delta\alpha$. Set t as τ , time axis ξ examined at any time corresponding to the state of Eqs. (10-11), its moment coefficients in accordance with Eq. (9) is $C_{m1}(t) = C_m(\alpha_1(\xi))$, $C_{m2}(t) = C_m(\alpha_2(\xi))$, the $\xi \leq t$. When $t > \tau$, $C_{m1}(t) \neq C_{m2}(t)$. If $\Delta C_m(t) = C_{m2}(t) - C_{m1}(t)$, if $\lim_{\substack{\Delta\alpha \rightarrow 0 \\ t > \tau}} \frac{\Delta C_m(t)}{\Delta\alpha}$, There is a unique limit, define this limit as an indicator function(indicial response):

$$A = \lim_{\substack{\Delta\alpha \rightarrow 0 \\ t > \tau}} \frac{\Delta C_m(t)}{\Delta\alpha} \tag{12}$$

For the Eq. (12), it is not difficult to conclude that aerodynamic moment coefficient difference $\Delta C_m(t)$ under the two kinds of t time is not only related to starting moment τ and observation time t , but also related to the $\Delta\alpha$ and attack angle α before τ :

$$\Delta C_m(t) = \Delta C_m[\alpha(\xi); \Delta\alpha, \tau, t] \quad -\infty \leq \xi \leq \tau \tag{13}$$

Based on Eq. (12):

$$A = A[\alpha(\xi); t, \tau] \quad -\infty \leq \xi \leq \tau \tag{14}$$

According to the definition of indicating function Eqs. (13-14), when $t > 0$, aerodynamic moment coefficient can be written as:

$$C_m(t) = C_m(0) + \int_0^t A[\alpha(\xi); t, \tau] \frac{d\alpha}{d\tau} d\tau \quad (0 \leq \xi \leq \tau) \tag{15}$$

The above equation is actually using the initial conditions: when $\tau < 0$, $\frac{d\alpha}{d\tau} = 0$. Therefore, Eq. (15) is response when aircraft flying from the benchmark when $\xi = 0$. That is to say, it represents the response of the aircraft when it begins a certain maneuvering action under the action of the control surface, or the transient process when the aircraft starts to deviate from the benchmark flight state under the action of disturbance.

To substitute the functional in Eq. (15) with ordinary function, we assume that $\alpha(\xi)$ could expand as Taylor series for convergence near the $\xi = \tau$, the Eq. (15) can be equivalent to write to:

$$A[\alpha(\xi); t, \tau] = A(t - \tau; \alpha(\tau), \dot{\alpha}(\tau), \ddot{\alpha}(\tau), \dots) \tag{16}$$

In the Eq. (16), $t - \tau$ appears alone by replacing t, τ , its physical meaning righteousness is clear, namely when $\tau, \alpha(\tau), \dot{\alpha}(\tau), \ddot{\alpha}(\tau), \dots$ is given, change history of $\alpha(\xi)$ has been given, the transient response $t - \tau$, rather than related with t, τ respectively. Therefore, Eq. (15) can be written as:

$$C_m(t) = C_m(0) + \int_0^t A(t - \tau; \alpha(\tau), \dot{\alpha}(\tau), \ddot{\alpha}(\tau), \dots) \frac{d\alpha}{d\tau} d\tau \tag{17}$$

According to the definition of the indicated response, when $t - \tau \rightarrow \infty$, indicial response $A(t - \tau; \alpha(\tau), \dot{\alpha}(\tau), \ddot{\alpha}(\tau), \dots)$ tends to rely on the constant of $\alpha(\tau)$, its limit is $A(\infty; \alpha(\tau))$. the deficiency function is defined as:

$$F(t - \tau; \alpha(\tau), \dot{\alpha}(\tau), \ddot{\alpha}(\tau), \dots) = A(\infty; \alpha(\tau)) - A(t - \tau; \alpha(\tau), \dot{\alpha}(\tau), \ddot{\alpha}(\tau), \dots) \tag{18}$$

When $t - \tau \rightarrow \infty$, $F \rightarrow 0$, substitute Eq. (18) into Eq. (17):

$$C_m(t) = C_m(\infty; \alpha(\tau)) - \int_0^t F(t - \tau; \alpha(\tau), \dot{\alpha}(\tau), \ddot{\alpha}(\tau), \dots) \frac{d\alpha}{d\tau} d\tau \tag{19}$$

As conversion $u = t - \tau$, Eq. (19) can be written as:

$$C_m(t) = C_m(\infty; \alpha(\tau)) - \int_0^t F(u; \alpha(t - u), \dot{\alpha}(t - u), \ddot{\alpha}(t - u), \dots) \frac{d\alpha(t - u)}{du} du \tag{20}$$

We have assumed that $\alpha(\xi)$ could expand as convergent Taylor series. While τ could be any point in $[0, t]$, so $\alpha(\xi)$ could expand as convergent Taylor series at any point in $[0, t]$. As $t - u = \tau \in [0, t]$, $\alpha(t - u), \dot{\alpha}(t - u), \ddot{\alpha}(t - u), \dots$ could expand as convergent Taylor series near t :

$$\begin{aligned} \alpha(t - u) &= \alpha(t) - \dot{\alpha}(t)u + \frac{\ddot{\alpha}(t)}{2}u^2 - \dots \\ \dot{\alpha}(t - u) &= \dot{\alpha}(t) - \ddot{\alpha}(t)u + \frac{\dddot{\alpha}(t)}{2}u^2 - \dots \\ \ddot{\alpha}(t - u) &= \ddot{\alpha}(t) - \dddot{\alpha}(t)u + \frac{\alpha^{(4)}(t)}{2}u^2 - \dots \end{aligned} \tag{21}$$

To substitute Eq. (21) into Eq. (20):

$$C_m(t) = C_m(\infty; \alpha(t)) + \sum_{i=1}^{\infty} C_i \frac{d^i \alpha(t)}{dt^i} \tag{22}$$

Among which

$$C_i = \frac{(-1)^{i+1}}{(i-1)!} \int_0^t F(u; \alpha(t), \dot{\alpha}(t), \ddot{\alpha}(t), \dots) u^{i-1} du \quad (i = 1, 2, 3, \dots) \tag{23}$$

Eq. (22), Eq. (23) is function relation between the aerodynamic moment coefficient $C_m(t)$ and the phase space variables when only angle of attack changes. By Eq. (23), it can be seen C_i is explicit function of t , namely $C_m(t)$ is not only the function of generalized state variables, but also implicit time t in the Eq. (24):

$$C_m(t) = C_m(\alpha(t), \dot{\alpha}(t), \ddot{\alpha}(t), \dots; t) \tag{24}$$

For general movement of all the state variables changes, aerodynamic force/moment coefficient expressions can also be analyzed, then ΔC_λ is related to aircraft motion parameters $(\alpha, \dot{\alpha}, \beta, \dots, Ma, h, u, v, \dots, \delta_e, \dot{\delta}_e)$. ΔC_λ is set as function of the state parameter in the Eq. (25):

$$\Delta C_\lambda(\alpha, \dot{\alpha}, \dots, \dot{\delta}_e) = \frac{\partial C_\lambda}{\partial \alpha} \Delta \alpha + \frac{\partial C_\lambda}{\partial \dot{\alpha}} \Delta \dot{\alpha} + \dots + \frac{\partial C_\lambda}{\partial \dot{\delta}_e} \Delta \dot{\delta}_e + H.O.T \tag{25}$$

By calculating the time domain data ΔC_λ dynamic derivative $\frac{\partial C_\lambda}{\partial \alpha}, \frac{\partial C_\lambda}{\partial \dot{\alpha}}, \dots, \frac{\partial C_\lambda}{\partial \dot{\delta}_e}$ is obtained by postprocess in The numerical methods include integral method, frequency domain transform method, regression method and phase method.

3. Study on the interference of the 7-degree blunt cone model dynamic derivative

3.1. Calculation model

The 7° blunt cone model is selected from the Arnold Engineering Development Center's Feng Kao Kamen Aerodynamics Laboratory (AEDC-VKF) 7 blunt cone support interference experiment [12]. AEDC's VKF wind tunnel forced pitching derivation test equipment is shown in Figure 1. The device uses a "Ten" word flexible pivot, a drive motor and a single-component torque beam. A strain gauge is attached to the single-component torque beam to measure the torque of the drive motor. The motor is connected to the connecting rod and the linkage and the torque beam. Coupling, the dynamic derivative test with amplitude of $\pm 2^\circ$ and frequency of 2~20Hz can be performed. The pitch angle displacement of the model is measured by the bending deformation of the "ten" flexible pivot. At the same time, the "Ten" flexible pivot can support the model and provide recovery torque, allowing the system to operate at a specific frequency. The unit is equipped with two "Ten" shaped flexible balances, each consisting of three structural beams with signal elements. The thickness of the balance beam is 0.087 and 0.171 in,

respectively, and the recovery torques can be -132 and -938ft•lb/rad, respectively. Different “Ten” flexible balances can be selected according to different aerodynamic loads during the test. In order to protect the balance, the model was held in place by a pneumatic spring-type locking device before and after the test. During the test, the model was released and the motor was driven to vibrate.

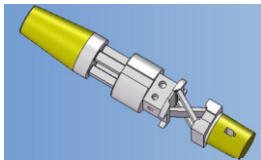


Figure 1. VKF wind tunnel forced pitching vibration balance structure diagram

The 7° blunt cone support interference experiment was derived from a three-year technical project to obtain the supporting interference characteristics of the system's supersonic and hypersonic wind tunnel experiments. The 7° blunt cone support interference experiment measures the influence of the tail support length on the dynamic derivative, the static pitching moment coefficient and the bottom pressure. At the same time, the factors such as Mach number, angle of attack, boundary layer flow state and reduction frequency are investigated in detail.

Figure 2 shows the dimensions and center of mass of the blunt cone. The experiment is divided into two different forms of support, as shown in Figure 3. The first type of support (Interference Sting, IS) strut length L_s is equal to the bottom diameter D length, so that there is strong interference between the support and the bottom flow field, and the second form of support (Clean Sting, CS) The length L_s of the strut is 3.3 times the diameter D of the bottom, and the interference effect is relatively weak due to the relatively long strut.

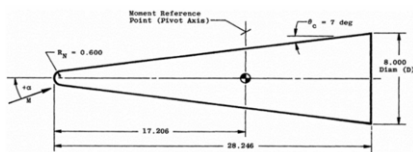


Figure 2. Blunt cone dimensions and centroid position

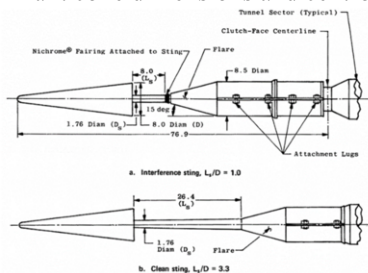


Figure 3. Two forms of support for the shape of a blunt cone

3.2. Effect of strut length on static aerodynamic forces

Figure 4 shows the experimental results of the pitch moment coefficients for different support forms under Mach number 2 and 8. As can be seen Under the condition of $Ma=8$, the length of the strut has little effect on the static pitching moment. The length of the strut has a slight influence on the static pitching moment under $Ma=2$. In this section, the static aerodynamic forces without support and different

strut lengths under Ma=5 are calculated and compared with experimental data. As shown in Figure 5, both the calculations and experimental results show that the length of the strut has little effect on the pitching moment. However, there is a difference of less than 5% between the calculation and the experiment. The greatest influence of support interference is the drag coefficient. The resistance coefficients of different strut lengths are different. Clean Sting is the closest to the unsupported calculation.

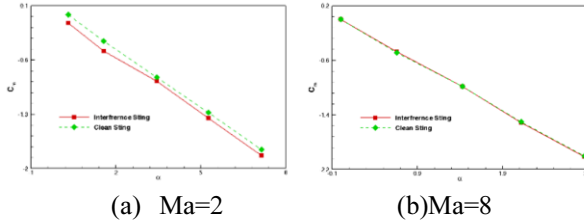


Figure 4. Comparison of Experimental Results of Pitch Coefficients with Different Support Forms

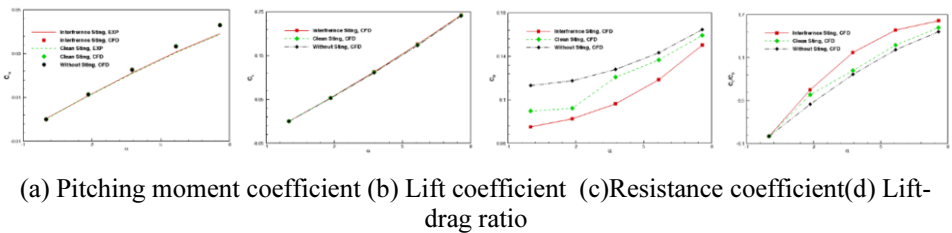


Figure 5. Comparison of aerodynamic/torque coefficient calculations and experimental results for different support forms

3.3. Influence of length of strut on dynamic derivative

Figure 6 shows the experimental results of the pitch moment coefficients for different support forms under Mach number 2 and 8. The difference in the thrust moment is that the pitch damping derivative under dynamic conditions is very different, and the maximum difference between the two can reach 40%. Figure 7 shows the calculation and experimental comparison of the pitch damping derivative for different support forms. Clean Sting and unsupported calculations are consistent in the trend before the 4° angle of attack, and the curves coincide above the 4° angle of attack. The length of the strut has a significant influence on the calculation results of the dynamic derivative. It can be seen that the support interference under dynamic conditions is far more complicated than under static conditions, and the support interference correction law under static conditions cannot be directly applied to dynamic unsteady conditions.

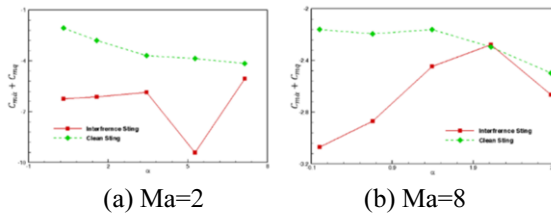


Figure 6. Comparison of Experimental Results of Pitch Damper Derivatives with Different Support Forms

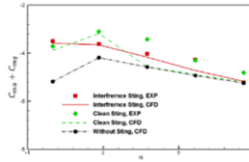


Figure 7. Comparison of Pitch Damper Derivative Calculation and Experiment with Different Support Forms

4. Conclusion

This paper studies the dynamic stability support interference of hypersonic vehicles based on the 7° blunt cone model, the transmission was carried out. The study of the support interference of the length of the rod is compared with the experimental data of the static aerodynamic force and the dynamic derivative. Three different support calculations were performed for the 7° blunt cone model. The length of the section D is equal, so that there is strong interference between the support and the bottom flow field. The length L_s is 3.3 times the diameter D of the bottom, and the interference effect is relatively weak due to the relatively long struts. The calculation results for static aerodynamics show that there is a difference of less than 5% between calculation and experiment. The length of the strut has little effect on the static pitching moment. The biggest influence of the supporting interference is the drag coefficient. The length of the strut is different. The coefficient of resistance is different, and Clean Sting is the closest to the calculation without support. The difference is that the pitch damping derivative under dynamic conditions is very different, and the maximum difference between the two can reach 40%. The calculation results of Sting and unsupported are consistent with the trend before the 4° angle of attack, and the curves are above the 4° angle of attack. The length of the strut has a significant influence on the calculation results of the dynamic derivative. It can be seen that the support interference under dynamic conditions is far more than static. Under the condition of state, the support interference correction law under static conditions cannot be directly applied to the dynamic unsteady condition.

References

- [1] Loeser T, Rohlf D. Experimental Determination of Dynamic Derivatives in a Wind Tunnel Using Parameter Identification. Springer International Publishing, 2016, doi:10.1007/978-3-319-27279-5_57.
- [2] Uselton J C, Uselton B L. Validity of Small-Amplitude Oscillation Dynamic-Stability Measurement Technique. Journal of Spacecraft & Rockets. 2015, 13: 266-270, doi:10.2514/3.57086.
- [3] Liu X, Liu W, Chai Z, Yang X. Research progress of numerical method of dynamic stability derivatives of aircraft. Acta Aeronautica Et Astronautica Sinica. 2016, 37: 2348-2369, doi: 10.7527/S1000-6893.2016.0098.
- [4] Mackay M A. Review of Sting Support Interference and Some Related Issues for the Marine Dynamic Test Facility (MDTF), 1993, Corpus ID: 107738918.
- [5] Ericsson L, Reding J. Review of support interference in dynamic tests. AIAA journal. 1983, 211: 1652-1666, doi: 10.2514/3.60166.
- [6] Taylor G, Gursul I. Support interference for a maneuvering delta wing. Journal of aircraft. 2005, 42: 1504-1515, doi: 10.2514/1.12094.
- [7] Yi BL, Zeng K, Wang S H. Investigation on the interference correction of flying wing aircraft rear sting support in high speed wind tunnel test. ACTA Aerodynamica Sinica. 2016, 34: 98-106, doi: 10.7638/kqdlxxb-2015.0098.

- [8] Mi B, Zhan H, Chen B. Calculating Dynamic Derivatives of Flight Vehicle with New Engineering Strategies. *International Journal of Aeronautical & Space Sciences*. 2017, 18: 175-185, doi:10.5139/IJASS.2017.18.2.175.
- [9] Zhang M, Dai J, Chen N. Transient dynamic stability test method for shock wind tunnel. *Journal of Electronic Measurement & Instrumentation*. 2016, 30:1812-1817, doi: 10.13382/j.jemi.2016.12.002.
- [10] Chikitkin A, Petrov M, Titarev V, Utyuzhnikov S. Parallel Versions of Implicit LU-SGS Method. *Lobachevskii Journal of Mathematics*. 2018, 39: 503-512, doi: 10.1134/S1995080218040054.
- [11] Pan J Z, Zhang J, Cai Y, Xu M. Investigation on the high-speed wind tunnel dynamic derivative test accuracy promotion. *ACTA Aerodynamica Sinica*. 2016, 34: 606-610, doi: 10.7638/kqdlxxb-2015.0110.
- [12] Useton B, Haberman D. Summary of sting interference effects for cone, missile, and aircraft configurations as determined by dynamic and static measurements. *Atmospheric Flight Mechanics Conference*, 1982, doi: 10.2514/6.1982-1366.